Computer Methods and Programs in Biomedicine 219 (2022) 106781

Contents lists available at ScienceDirect

Computer Methods and Programs in Biomedicine

journal homepage: www.elsevier.com/locate/cmpb

Estimation of central pulse wave velocity from radial pulse wave analysis

Yang Yao[a,b], Shuran Zhou[b], Jordi Alastruey[c,d], Liling Hao[b], Stephen E. Greenwald[e], Yuelan Zhang[f], Lin Xu[a], Lisheng Xu[b,g,*], Yudong Yao[h]

[a] School of Information Science and Technology, ShanghaiTech University, Shanghai, 201210, China
[b] College of Medicine and Biological Information Engineering, Northeastern University, Shenyang, Liaoning 110169, China
[c] Department of Biomedical Engineering, King's College London, London SE1 7EH, United Kingdom
[d] World-Class Research Center, "Digital Biodesign and Personalized Healthcare", Sechenov University, Moscow, Russia
[e] Blizard Institute, Barts & The London School of Medicine and Dentistry, Queen Mary University of London, London, United Kingdom
[f] The First Hospital of China Medical University, Shenyang, Liaoning 110122, China
[g] Neusoft Research of Intelligent Healthcare Technology, Co. Ltd., Shenyang, Liaoning 110169, China
[h] Department of Electrical and Computer Engineering, Stevens Institute of Technology, Hoboken, NJ, United States of America

ARTICLE INFO

Article history:
Received 17 October 2021
Revised 13 March 2022
Accepted 26 March 2022

Keywords:
Arterial stiffness
Pulse wave analysis
Pulse wave velocity
Wave separation analysis

ABSTRACT

Background and Objective: Arterial stiffness, commonly assessed by carotid-femoral pulse wave velocity (cfPWV), is an independent biomarker for cardiovascular disease. The measurement of cfPWV, however, has been considered impractical for routine clinical application. Pulse wave analysis using a single pulse wave measurement in the radial artery is a convenient alternative. This study aims to identify pulse wave features for a more accurate estimation of cfPWV from a single radial pulse wave measurement.

Methods: From a dataset of 140 subjects, cfPWV was measured and the radial pulse waveform was recorded for 30 s twice in succession. Features were extracted from the waveforms in the time and frequency domains, as well as by wave separation analysis. All-possible regressions with bootstrapping, McHenry's select algorithm, and support vector regression were applied to compute models for cfPWV estimation. *Results:* The correlation coefficients between the measured and estimated cfPWV were $r = 0.81$, $r = 0.81$, and $r = 0.8$ for all-possible regressions, McHenry's select algorithm, and support vector regression, respectively. The features selected by all-possible regressions are physiologically interpretable. In particular, the amplitude ratio of the diastolic peak to the notch of the radial pulse waveform ($\boldsymbol{R}_{n,d}^{r,P}$) is shown to be correlated with cfPWV. This correlation was further evaluated and found to be independent of wave reflections using a dataset ($n = 3{,}325$) of simulated pulse waves.

Conclusions: The proposed method may serve as a convenient surrogate for the measurement of cfPWV. $\boldsymbol{R}_{n,d}^{r,P}$ is associated with aortic pulse wave velocity and this association may not be dependent on wave reflection.

1. Introduction

Aortic stiffness is independently associated with cardiovascular events, target organ damage, and all-cause mortality [1,2]. When added to standard risk factors (e.g., blood pressure), aortic stiffness improves the prediction of cardiovascular events [3]. Carotid-femoral pulse wave velocity (cfPWV) has been proposed as the noninvasive gold standard for assessing aortic stiffness [4–6]. However, its measurement requires a skilled operator and remains confined to specialist centers. Besides, the carotid-femoral distance is hard to estimate accurately in obese patients. Thus, the measurement of cfPWV is not recommended for routine practice [7].

Pulse wave analysis is an alternative technique to assess arterial stiffness using a single arterial pressure waveform. The augmentation index (AIx) calculated from the radial pulse waveform or the synthetized aortic pulse waveform computed from the radial pulse waveform has been suggested as an index of stiffness [8]. However, several influencing factors (e.g., body height and heart rate (HR)) limit its performance [8]. In addition, the calculation of AIx is not reliable enough in some subjects due to the difficulty in determining the second peak of the radial pulse waveform or the in-

Abbreviations: cfPWV, carotid-femoral Pulse Wave Velocity; AIx, augmentation index; WSA, wave separation analysis; SEVR, sub-endocardial variability ratio; RM, reflection magnitude; RI, reflection index; BMI, body mass index; HR, heart rate; ICC, intra-class correlation.

* Corresponding author at: Northeastern University, China.
E-mail address: xuls@bmie.neu.edu.cn (L. Xu).

https://doi.org/10.1016/j.cmpb.2022.106781
0169-2607/

flection point of the aortic pulse waveform. In recent years, wave separation analysis (WSA) based on an approximated flow wave has been used to assess arterial stiffness, by calculating the pulse transit time as the time delay between the forward wave and the backward-traveling reflected wave [9]. However, this delay is determined not only by the speed of the pulse but also by the distance it travels, i.e. the effective reflection distance (distance from an aortic measurement site to a notional site from which all distal reflections appear to originate), which is influenced by several factors like the length of the arterial tree and central-to-peripheral arterial stiffness gradient [10].

This study aims to investigate the pulse wave features that allow an accurate estimation of cfPWV from a single pulse wave measurement in the radial artery. We firstly extracted a set of features from the radial and derived aortic pulse waveforms (using a transfer function [11]) and identified those that enable accurate cfPWV estimation. The associations of these identified features with aortic stiffness were further confirmed using a dataset of simulated pulse waves in 3325 virtual subjects.

2. Methods

2.1. Subjects and experimental protocol

This study was conducted in 2020–2021 at the Northeastern University, China, and was approved by the Biological and Medical Ethics Committee of the university (No. NEU-EC-2020B017S; date of approval: 2020.11.20). A total of 149 volunteers were recruited. The volunteers were all Chinese, comprising students and faculty members of the university, as well as residents from nearby communities. All subjects gave their informed consent. The sample size was calculated using the G*Power software [12,13] (effect size f^2=0.33 which was determined from the prior knowledge that a pulse wave feature such as the travel time of the reflected wave from a central artery site to a peripheral reflecting site and back, has been reported to be associated with cfPWV with an absolute correlation coefficient of over 0.5 [14], α=0.05, power 1-β=0.80, number of predictors =15), giving a suggested minimum sample size of 70. Data from nine subjects were excluded due to lack of evident feature points (inflection points and/or notch) in the derived aortic pulse waveform, resulting in a set of 140 subjects (69 males and 71 females; age, 47±21 years; height, 166±9 cm; weight, 65±11 kg). Table 1 lists their cardiovascular status.

As shown in Fig. 1, after a 5 min rest, blood pressure was measured in each subject while seated. Subjects remained in a supine position thereafter. After a further 2 min rest, right carotid and femoral pulse waveforms were simultaneously recorded twice (for at least 30 s. each time) using two pulse sensors (MP100, Xinhangxingye Co. Ltd., China). Signals were sampled at 1 kHz with a BL-420S data acquisition system (Chengdu Techman Software Co. Ltd, China). Then the straight-line distance between the right carotid and femoral artery sites was measured with a tape to the nearest half centimeter. Immediately following this, the radial pulse waveform was recorded twice, for 10 s each time, using a sphygmomanometer (SphygmoCor, AtCor, Australia; sampling at 128 Hz).

Table 1
Cardiovascular Status of the Subjects.

# subjects	Cardiovascular abnormality and/or disease
2	Premature left ventricular contraction
2	Arrhythmia
6	Hypertension
1	Arteriosclerosis
1	Abnormal mitral regurgitation
2	Myocardial ischemia
1	Coronary heart disease
1	Cerebral infarction and arteriosclerosis
1	Left ventricular insufficiency and atrial fibrillation
1	Hypertension and arrhythmia
1	Arrhythmia, coronary heart disease, and hypothyroidism
3	Renal disease
3	Hypertension and renal disease
115	No cardiovascular abnormality or disease reported

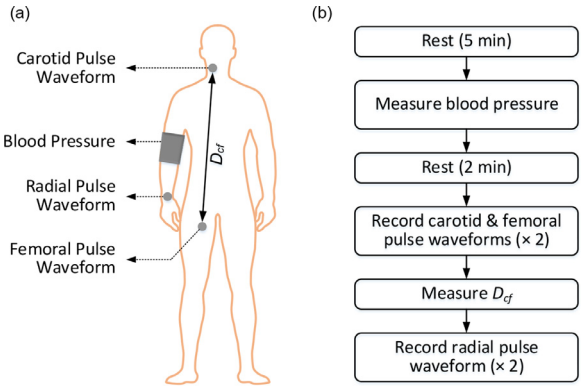

Fig. 1. Experimental details: (a) Signal acquisition; (b) Experimental protocol. D_{cf}: carotid-femoral distance. ' × 2' means two successive measurements.

2.2. Calculation of pulse wave velocity

The carotid and femoral pulse signals were processed by removing the baseline drift and noise via wavelet decomposition. More specifically, the baseline was calculated as the approximation layer of a 10-level 'sym7' wavelet decomposition [15,16]. The noise was approximated by the detail layer of a 4-level 'db7' wavelet decomposition [15,16].

In each subject, cfPWV was calculated from each of the two simultaneous recordings of carotid and femoral pulse waveforms as suggested by the expert consensus documents [4,5]. For each cardiac period, the respective feet of the carotid and femoral pulse signals were determined by the intersecting tangent method [17,18]. The carotid-femoral pulse transit time was taken as the time difference between the feet of the carotid and femoral pulse waveforms. Then, the cfPWV was calculated as 0.8 times the carotid-femoral distance divided by the pulse transit time [5]. For each subject, a representative value was derived from the beat-by-beat cfPWVs by: (1) calculating the average over all beats in each of the two recordings, and (2) taking the mean of these two average values.

2.3. Pulse wave analysis

For the two simultaneous measurements in each subject, a series of synthetized aortic pressure waveforms were derived from the SphygmoCor device using the transfer function method [11]. A representative pulse waveform was generated from each time series of the radial and aortic pulse waveforms, by means of the ensemble averaging technique embedded in the device's software. Several features were extracted from the representative radial and aortic pulse waveforms in the time and frequency domains, as well as by applying WSA to the aortic pulse waveforms (see appendix for details).

In the time domain, features were calculated based on the timing and amplitude of several fiducial points (Fig. 2). In the aortic pressure waveform, the timing of the foot indicates the opening of the aortic valve and the start of blood injection. Therefore, the foot corresponds to the diastolic blood pressure in the aorta. The inflection point is associated with wave reflections [19]. The peak

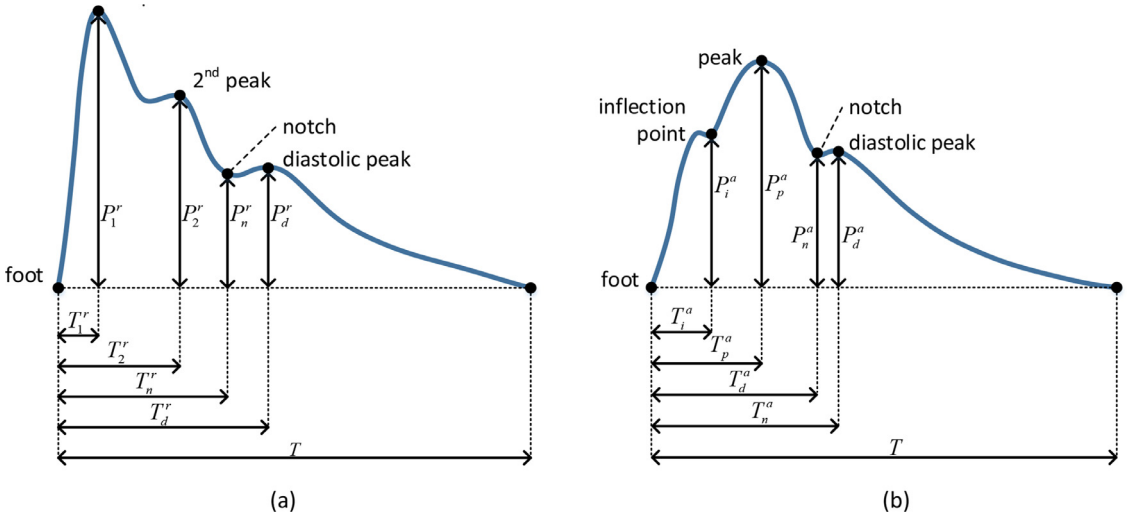

Fig. 2. Extraction of feature points from (a) radial and (b) aortic pulse waveforms.

marks the highest pressure generated by the heart to drive blood from the central aorta to the periphery. The notch corresponds to where the aortic valve closes and, in a healthy circulation, when the ejection of blood from the left ventricle stops. In the radial pressure waveform, the foot and the notch share the same physiological meaning as in the aortic pressure waveform. The first peak, formed by the aortic forward wave traveling to the radial artery, marks the local systolic blood pressure. The second peak is associated with wave reflections [8]. The diastolic peak has not been widely investigated but was found to provide additive value in estimating cfPWV from the radial pulse waveform in one of our previous studies [20].

The determinations of the foot and notch of the radial and derived aortic pulse waveform were performed using the same method: the foot was determined by the intersecting tangent technique; the notch was identified as the local maximum of the second derivative. For the radial pulse waveform, the first peak was taken as the global maximum. The second peak was identified as the local peak of the measured wave or the local minimum of its second derivative following the first peak. The diastolic peak was identified as the local maximum of the measured wave or the local minimum of its second derivative after the notch. For the derived aortic pulse waveform, the peak was taken as the global maximum. The inflection point was determined as the second peak of the second derivative following the foot, or the local maximum of the second derivative after the peak [21].

The timing and amplitude of the first peak, second peak, notch, and diastolic peak with respect to the foot were defined as T_1^r, T_2^r, T_n^r, T_d^r and P_1^r, P_2^r, P_n^r, P_d^r, respectively. The time difference between the first and second peak (T_{12}^r) was calculated as $T_2^r - T_1^r$, which may be associated with aortic stiffness since the first and second peaks are generated mainly by the aortic forward and backward pressure waves from the lower body, respectively. The time ratios $R_{1,n}^{r,T} = T_1^r/T_n^r * 100\%$, $R_{2,n}^{r,T} = \frac{T_2^r}{T_n^r} * 100\%$, as well as $R_n^{r,T} = T_n^r/T * 100\%$, were also calculated. The radial augmentation index and diastolic augmentation index were defined as $AI^r = P_2^r/P_1^r * 100\%$ and $AI_d^r = P_d^r/P_1^r * 100\%$, respectively. The amplitude ratios defined as $R_{n,1}^{r,P} = P_n^r/P_1^r \times 100\%$ and $R_{d,n}^{r,P} = P_d^r/P_n^r \times 100\%$ were also included for feature selection.

Similarly, the timing and amplitude of the peak, inflection point, and notch with respect to the foot of the central aortic pulse waveform were defined as T_p^a, T_i^a, T_n^a and P_p^a, P_i^a, P_n^a, respectively. The time difference between the peak and inflection point was calculated as $T_{p,i}^a = |T_p^a - T_i^a|$, since they are associated with the forward and backward wave, respectively. The diastolic duration was calculated as $T_{dia}^a = T - T_n^a$. Several time ratios were calculated, i.e., $R_{1,n}^{a,T} = T_1^a/T_n^a \times 100\%$, $R_{2,n}^{a,T} = T_2^a/T_n^a \times 100\%$, $R_n^{a,T} = T_n^a/T \times 100\%$, and $R_{dia}^{a,T} = T_{dia}^a/T \times 100\%$. Aortic augmentation index was defined as $(P_p^a - P_i^a)/P_p^a \times 100\%$ if the inflection point appeared before the peak, and $-(P_p^a - P_i^a)/P_p^a \times 100\%$ if the inflection point appeared after the peak. The amplitude ratio between the notch and the peak was calculated ($R_n^{a,P} = P_n^a/P_p^a \times 100\%$), but not between diastolic peak and notch, since a diastolic peak was hardly visible in some subjects. Sub-endocardial variability ratio (SEVR), also known as Buckberg index [22] for assessing subendocardial perfusion, was calculated from the aortic pressure waveform as the area under the curve between the foot and the following notch divided by that between the notch and the following foot.

Frequency-domain features were calculated from the time series of the radial and derived aortic pulse waveforms. After calculation of the frequency spectrum using the fast Fourier transform, the second to the fifth peak amplitudes normalized by the first peak amplitude (H_2^a/H_1^a, H_3^a/H_1^a, H_4^a/H_1^a, and H_5^a/H_1^a for radial pulse waveforms; H_2^r/H_1^r, H_3^r/H_1^r, H_4^r/H_1^r, and H_5^r/H_1^r for aortic pulse waveforms) were included as features in the subsequent analysis, given that the first 5 harmonics of the discrete Fourier series are sufficient to represent most of the variance in radial or aortic pulse waveforms [21].

WSA can be used to assess arterial stiffness because the stiffness of the arteries determines how fast the pulse wave travels along them and the stiffness gradient affects where and to what extent the pulse wave is reflected [23]. Therefore, both the timing and amplitude features from the forward and backward waves are associated with arterial stiffness. WSA based on the aortic pressure waveform alone[24], as first proposed by Westerhof et al. [25], was applied to the representative derived aortic pulse waveform. This method approximates the flow waveform by a triangular wave, with duration equal to the ejection duration and peak flow timing equal to that of the inflection point. This 'triangular flow' assumption may sometimes result in large backward wave before the inflection point or sharp forward and backward waves. Following Qasem and Avolio [9], we made a correction by assuming that no reflected wave occurred before the inflection point and maintaining the backward wave amplitude constant from the foot to the inflection point. The time delay (T_{fb}) between the forward and backward wave was calculated by cross-correlation, again following Qasem and Avolio [9]. Reflection magnitude (RM) was calculated as the ratio of the backward wave amplitude to the forward wave

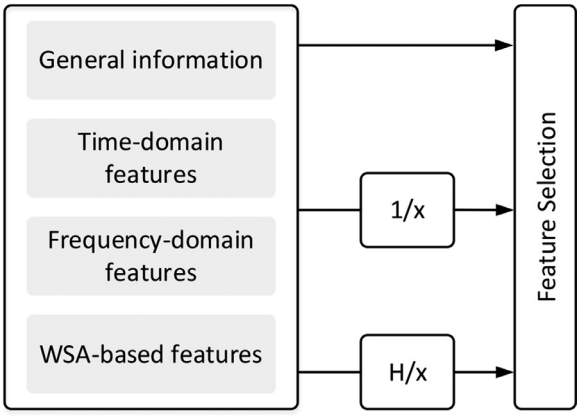

Fig. 3. Feature generation. Three sets of features were included in the selection process: (1) the raw features including subjects' general information and those extracted from the time-domain, frequency-domain, and wave separation analysis (WSA); (2) the reciprocal of all the raw features; (3) all the reciprocals multiplied by the body height, *H*. '1/x' indicates taking the reciprocal. '*H*/x' indicates multiplying the height after taking the reciprocal.

amplitude [26]. Reflection index (RI) was calculated as the ratio of the amplitude of the backward wave to the sum of the amplitudes of the forward and backward waves [26]. The determination of the second peak of the radial pulse waveform or the inflection point of the aortic pulse waveform has been shown to be challenging in some subjects. For a more clinically applicable alternative, the timing of peak flow is sometimes determined as 30% of the ejection duration. Both methods were applied in this study. T_{fb30}, RM_{30}, and RI_{30} were T_{fb}, RM, and RI calculated based on this assumption, respectively.

2.4. Modeling and validation

Features calculated in the time and frequency domains, as well as from WSA were all considered candidates for cfPWV estimation. Some general information about the subjects was also included. Specifically, the characteristics entered into the feature selection analysis were: gender (*G*), height (*H*), weight (*W*) and body mass index (BMI). As mentioned previously, the clinical significance of cfPWV is its independent and additive value for predicting cardiovascular events over and above conventional risk factors such as age and blood pressure. Thus, age, as well as blood pressure-related features from pulse wave analysis, were not considered in the feature selection. The cardiac period (*T*), HR, calculated as 60/*T*, and pulse pressure ratio between radial and aortic pulse waveform, were also included in the feature selection.

Many of the above calculated features may be related to the pulse transit time (e.g., the timing features and reflection-related features) and their reciprocals, therefore, to pulse wave velocity. As shown in Fig. 3, we generated a set of new features by taking the reciprocal of all the features except for gender, height, cardiac period, and HR. Note that we used 1-AI^a instead of AI^aduring this procedure, since AI^a may be zero, and its reciprocal could, therefore, go to infinity. Another set of new features was generated by multiplying the above reciprocals by *H*, assuming that *H* is positively correlated with pulse transit distance.

The agreement between the two measurements of cfPWV and features from the radial and aortic pulse waveforms was assessed by intra-class correlation (ICC; two-way random effects, absolute agreement, single rater) [27–29]. All features with ICC<0.75 were excluded from subsequent analysis.

The relationship between the features associated with the radial and derived aortic pulse waveforms and cfPWV was investigated through all-possible regressions with bootstrapping. Specifically, every possible combination of the features was entered into a regression model and the ones that better estimated cfPWV (in terms of correlation coefficient) were selected. This process was repeated 100 times by randomly sampling the data with replacement and the correlation coefficients derived were averaged. However, this exhaustive bootstrapping regression becomes computationally expensive as the number of features included in the regression model increases. Therefore, we stopped increasing the number of features to include in the regression models at 4 for all-possible regression analysis, and employed the McHenry's select algorithm, which produces a similar performance with much lower computational cost, as an attempt to include more features in the regression model and improve the estimation performance [30]. Furthermore, ν-support vector regression with gaussian kernel was also applied to estimate cfPWV. The features were normalized to zero mean and unit standard deviation before modeling. ν was set as 0.5. The hyperparameters were optimized by 5-fold cross-validated grid-search, with ranges being $[10^{-3}, 10^{12}]$ for the cost, $[10^{-3}, 10^{12}]$ for the kernel scale. To test the above methods, the dataset was split into a training set ($N = 90$) and a test set ($N = 50$). Each of the models were computed based on the training set and validated on the test set. In particular, the hyperparameters for support vector regression were tuned on the training set. The features in the training set were normalized; while the features in the test set were not normalized, but scaled by the mean and standard deviation of the training set.

2.5. Numerical study

The association of pulse wave features with aortic stiffness was further confirmed and investigated using a dataset of simulated pulse waves in thousands of virtual subjects. This dataset was generated by a one-dimensional (1-D) model of blood flow in the 55 larger arterial segments of the human systemic circulation. The cardiac and arterial variables of the model are listed in Table 2, along with their variations, each expressed as a multiple of the baseline value. These variations of seven basic variables give a set of 7776 cases, which was reduced to 3325 cases with rejection criteria. Further details can be found in a previous study [31].

The definitions of all features in the simulated radial and aortic pulse waves are the same as in the measured pulse waves, while the extraction of the foot and dicrotic notch as well as the wave separation procedure differs. In the measured radial and aortic pulse waves, the foot was extracted via the intersecting tangent method. In the numerical study, the foot of the radial and aortic pulse waveform was simply defined as the local minimum in late diastole. The dicrotic notch was defined as the point 0.31 s after the foot, due to the fact that the ejection period was set to 0.31 s. Furthermore, wave separation was applied to the aortic and radial pulse waveform based on the model-generated flow velocity instead of the triangular approximation of the flow wave used for the in vivo data, along with the local pulse wave velocity [32]. The

Table 2
Basic hemodynamic variables and the corresponding multiplication factors in the computational model.

Variables	Symbol/ Abbreviation	Multiplication factor (%)
Elastic arteries PWV	$\boldsymbol{c_e}$	81, 100, 130, 160, 190, 225
Muscular arteries PWV	$\boldsymbol{c_m}$	80, 100, 115, 130
Elastic arteries diameter	$\boldsymbol{D_e}$	90, 100, 120, 140
Muscular arteries diameter	$\boldsymbol{D_m}$	90, 100, 121
Heart rate	HR	85, 100, 115
Stroke volume	SV	80, 100, 120
Peripheral vascular resistance	PVR	90, 100, 110

forward (P_f) and backward (P_b) pressure waveform can be calculated using the following equations,

$$dP_f = \frac{1}{2}(dP + \rho c dU) \tag{1}$$

$$dP_b = \frac{1}{2}(dP - \rho c dU) \tag{2}$$

where ρ is the blood density, c represents the pulse wave velocity, P and U are the pressure waveform and the flow velocity waveform, respectively.

Local sensitivity analysis was employed to quantify the association of $R^{r,P}_{n,d}$ with aortic PWV (as measured by c_e), as well as other hemodynamic parameters (c_m, D_e, D_m, HR, SV, PVR) in 1-D model. As a comparison, the effect of the hemodynamic variables on cfPWV, RM, and T_{fb} was also analyzed using local sensitivity analysis.

The sensitivity of a pulse wave feature y to a basic hemodynamic variable x was defined as

$$I_i(x_1, \cdots, x_n) = \frac{\Delta y}{y_{max} - y_{min}} \frac{x_{max} - x_{min}}{\Delta x_i} \tag{3}$$

where Δy means the change in y due to the change in x_i when other basic hemodynamic variables x_j ($j \neq i$) remain constant. The subscripts 'max' and 'min' indicate global maximum and minimum across the dataset, respectively.

Most of the pulse wave features that correlate with aortic stiffness are associated with pulse wave reflection. Therefore, we went a step further to investigate the relationship between wave reflection and the association between $R^{r,P}_{n,d}$ and aortic stiffness. The amplitude ratio between the diastolic peak and the notch from both the whole radial pulse waveform (i.e., $R^{r,P}_{n,d}$) and its corresponding forward pulse waveform (denoted as $R^{rf,P}_{n,d}$) was calculated. A comparison between the sensitivity of $R^{r,P}_{n,d}$ and $R^{rf,P}_{n,d}$ versus the hemodynamic variables of the 1-D model was applied. Additionally, the correlation coefficient between $R^{r,P}_{n,d}$ and $R^{rf,P}_{n,d}$ was calculated. If the association of $R^{r,P}_{n,d}$ with aortic stiffness is dependent on wave reflection, the sensitivity of $R^{rf,P}_{n,d}$ should not follow that of $R^{r,P}_{n,d}$ and the correlation between the two should be poor. The same definition (deriving $R^{a,P}_{n,d}$ and $R^{af,P}_{n,d}$) and analysis was applied to the aortic pressure wave, as a comparison for $R^{r,P}_{n,d}$ and $R^{rf,P}_{n,d}$.

3. Results

The HR difference between the measurements derived from carotid/femoral and radial pulse waveforms was: -1 ± 5 bpm. The difference between the two repeated measurements of cfPWV was 0 ± 0.3 m/s, and the ICC was 0.99. In the ICC analysis, 68/127 of the features gave an ICC of ≥ 0.9; 25/127 gave an ICC of ≥ 0.75; and 28/127, ≥ 0.5. 6/127 of the features gave ICC values < 0.5. These were: $R^{r,H}_{2,1}$, $1/R^{r,P}_{n,1}$, $1/R^{r,H}_{2,1}$, $H/R^{r,P}_{n,1}$, $H/R^{r,H}_{2,1}$, $R^{r,P}_{d,n}$. Thus, 93/127 features were included for feature selection, these being the ones giving ICC values ≥ 0.75.

For all-possible regressions, including $N = 1$ to 4 features in the regression model gave correlation coefficients of $r = 0.75$, $r = 0.78$, $r = 0.79$, and $r = 0.81$ between the estimated and measured cfPWV, respectively. The selected feature/feature pairs were $1/T_{fb}$ for $N = 1$, $1/T_{fb}$ and $1/T^r_d$ for $N = 2$, $1/T_{fb}$, $1/T^r_d$, and $1/W$ for $N = 3$, $1/T^r_d$, $1/W$, RI, and AI^r_d for $N = 4$. Fig. 4 shows the cross-validation result for the best regression model with $N = 4$ independent variables. The estimation errors were 0 ± 1.2, -0.1 ± 1.2, -0.1 ± 1.2, and -0.1 ± 1.1 m/s for $N = 1$ to 4, respectively. The top 10 features/feature pairs for the univariate ($N = 1$) regression models are listed in Table 3, along with the corresponding correlation coefficients between the estimated and measured cfPWV. The conventional AIx (AI^a and AI^r) derived correlations were $r = 0.59$ and $r = 0.58$ between the estimated and measured cfPWV, respectively (not listed in the table).

Fig. 5 shows the correlation coefficients between the measured and the estimated cfPWV from features ($N = 1$–10) selected using the McHenry's select algorithm during validation. Fig. 6 is a comparison of the measured and the estimated cfPWV when $N = 5$ features were selected via McHenry's select algorithm during validation. Fig. 7 shows a comparison of the measured and estimated cfPWV by support vector regression during validation.

Fig. 8 shows the sensitivity of cfPWV, RM, T_{fb} and $R^{r,P}_{n,d}$ versus several basic hemodynamic variables. Each blue bar represents the mean sensitivity value of a pulse wave feature (or cfPWV) for one of the basic hemodynamic variables. The error bars are $\pm$ SD. Fig. 9 presents spider plots of cfPWV, RM, T_{fb} and $R^{r,P}_{n,d}$, when all multiplication factors for the basic hemodynamic variables of the 1-D model are set equal to 100%. Each line indicates the change of a pulse wave feature (or cfPWV) with one of the basic hemodynamic variables when the others are kept constant (i.e., multiplication factors equal 100%).

Similarly, Fig. 10 shows the sensitivity comparison of $R^{r,P}_{n,d}$, $R^{rf,P}_{n,d}$, $R^{a,P}_{n,d}$ and $R^{af,P}_{n,d}$ versus basic hemodynamic variables. Fig. 11 presents spider plots of $R^{r,P}_{n,d}$, $R^{rf,P}_{n,d}$, $R^{a,P}_{n,d}$ and $R^{af,P}_{n,d}$, when all multiplication factors for the basic hemodynamic variables of the 1-D model equal 100%. Fig. 12 presents the correlation analysis between $R^{r,P}_{n,d}$ and $R^{rf,P}_{n,d}$.

4. Discussion

cfPWV is the current standard technique for determining arterial stiffness. However, it is generally considered impractical for routine clinical assessment and its use is therefore confined to specialist centers. This study investigated the estimation of cfPWV based on a single easily accessible pulse wave, recorded at the radial artery, as a step towards developing an accurate and easy to use alternative.

4.1. Validity of the experimental data

The reliability of the cfPWV measurement is substantiated by the fact that: (1) the cardiovascular status of the subjects did not change appreciably during the two measurements (HR change: -1 ± 5 bpm); (2) the repeated measurements of cfPWV were close (difference: 0 ± 0.3 m/s; ICC=0.99). The derived radial pulse waveform was validated by a signal quality index embedded in the SphygmoCor device. Most of the pulse wave features showed

Table 3
Feature selection: Top 10 regression models with $N = 1$ independent variable.

Ranking	1	2	3	4	5	6	7	8	9	10
Feature	H/T_{fb}	$1/T_{fb}$	$1/T_{fb30}$	H/T_{fb30}	RM_{30}	$\boldsymbol{T^r_{12}}$	RI_{30}	$\boldsymbol{HR^{r,P}_{n,d}}$	$\boldsymbol{R^{r,P}_{n,d}}$	$1/\boldsymbol{T^r_{12}}$
r	0.75	0.75	0.71	0.68	0.66	0.66	0.66	0.66	0.65	0.65

r: correlation coefficient between estimated and measured cfPWV; $R^{r,P}_{n,d}$ is the reciprocal of $R^{r,P}_{d,n}$. This notation is used hereafter.

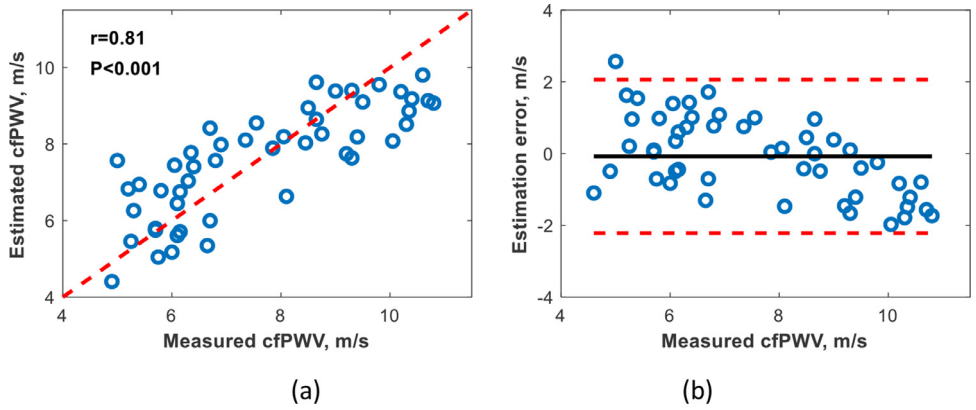

Fig. 4. Validation of the best feature combination selected when including $N = 4$ features in the regression model. (a) scatter plots of measured versus estimated carotid-femoral pulse wave velocity; (b) Bland-Altman plot of the measured versus estimated carotid-femoral pulse wave velocity.

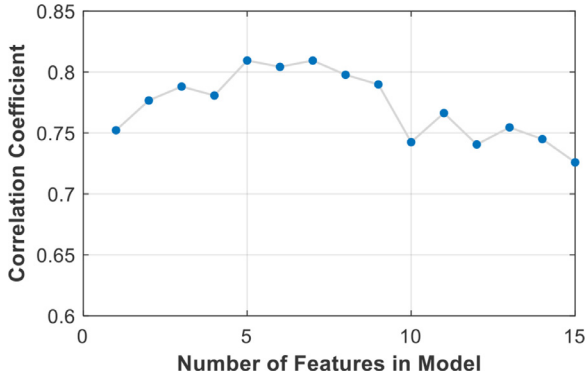

Fig. 5. Performance of the features selected via McHenry's select algorithm: correlation coefficients between estimated and measured cfPWV when the number of features ranges from 1 to 10.

good repeatability (121/127 of them yielded ICC values of ≥ 0.5). Poor agreement (ICC<0.5) between the two measurements was found only in the remaining 6/127 features. Possible reasons are: (1) some of the feature points (e.g., the second peak of the radial pulse waveform) were hard to extract reliably from the waveforms in some subjects (e.g., $R^{r,H}_{2,1}$, $1/R^{r,H}_{2,1}$, $H/R^{r,H}_{2,1}$); (2) multiplying and/or reciprocal operations enlarged the difference between measurements (e.g., $1/R^{r,P}_{n,1}$, $H/R^{r,P}_{n,1}$, $R^{r,P}_{d,n}$). These features should be avoided in clinical assessment of arterial stiffness, even if they are physiologically relevant. In this paper, as mentioned above, only features with ICC>0.75 ($n = 90$) were included in the subsequent analysis.

4.2. Physiological relevance of the selected features

The features selected in the univariate regression analysis were interpretable and corresponded well with the findings in previous studies [8,9]. WSA-related timing features H/T_{fb} and $1/T_{fb}$ yielded the best estimation of cfPWV ($r = 0.75$ for both). The approximation of these two features, H/T_{fb30} and $1/T_{fb30}$, also gave good performance ($r = 0.68$ and $r = 0.71$, respectively). A plausible explanation is that T_{fb}, which represents the time for the pressure wave to travel from the aorta to the lower body and back, is, to a large extent, determined by the stiffness of the artery through which the pressure wave passes (e.g., thoracic and abdominal aorta), as well as their combined length [33,34]. This supports the findings of Qasem and Avolio [9] and also the recommendation from the statement of the American Heart Association [6] that WSA should be applied when assessing wave reflection. WSA-related amplitude features, which represent the magnitude of the reflected wave, also correlated well with cfPWV (e.g., RM_{30} and RI_{30} both with $r = 0.67$). This is consistent with prior studies [35–37]. Possible reasons might be that the effect of wave attenuation is greatly reduced as the artery stiffens, although an increase in central arterial stiffness, for instance due to aging, cancels out the stiffness mismatch between the central and peripheral arteries, thereby lowering wave reflection [23]. T^r_{12} (and $1/T^r_{12}$) was selected because the first and second peaks are generated respectively by the forward traveling wave and the one that travels from the aorta to the lower

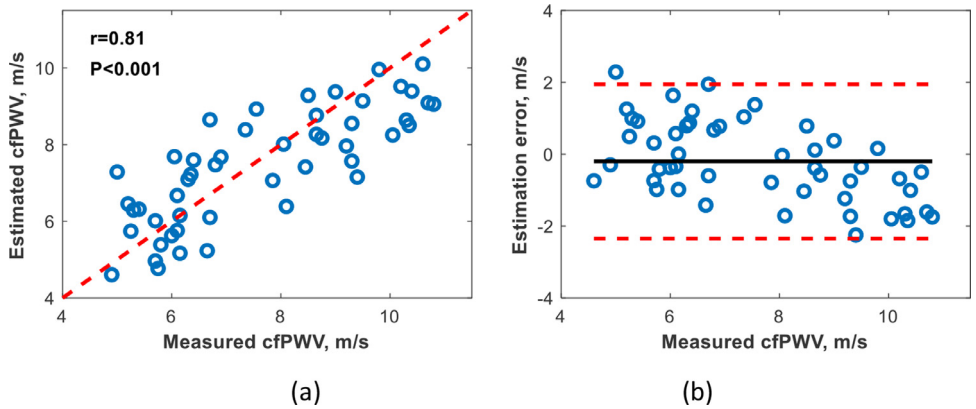

Fig. 6. Performance of the features selected via McHenry's select algorithm with $N = 5$ features included in the regression model. (a) scatter plots of measured versus estimated carotid-femoral pulse wave velocity; (b) Bland-Altman plot of the measured versus estimated carotid-femoral pulse wave velocity.

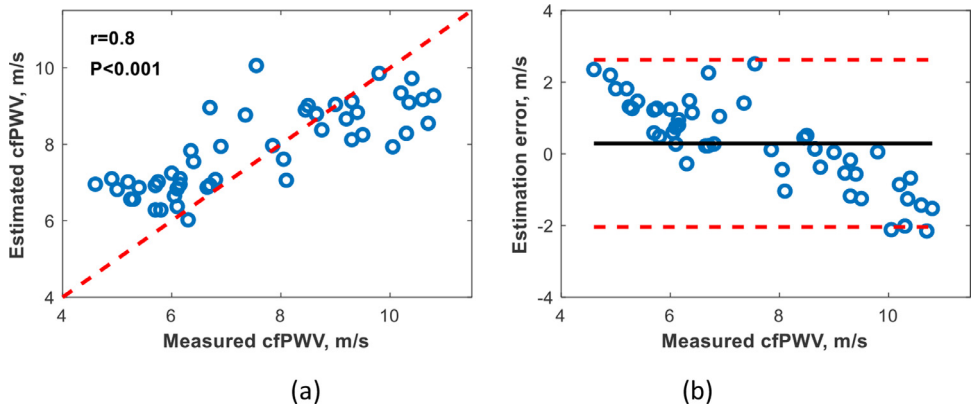

Fig. 7. Performance of the support vector regression method for the estimation of carotid-femoral pulse wave velocity. (a) scatter plots of measured versus estimated carotid-femoral pulse wave velocity; (b) Bland-Altman plot of the measured versus estimated carotid-femoral pulse wave velocity.

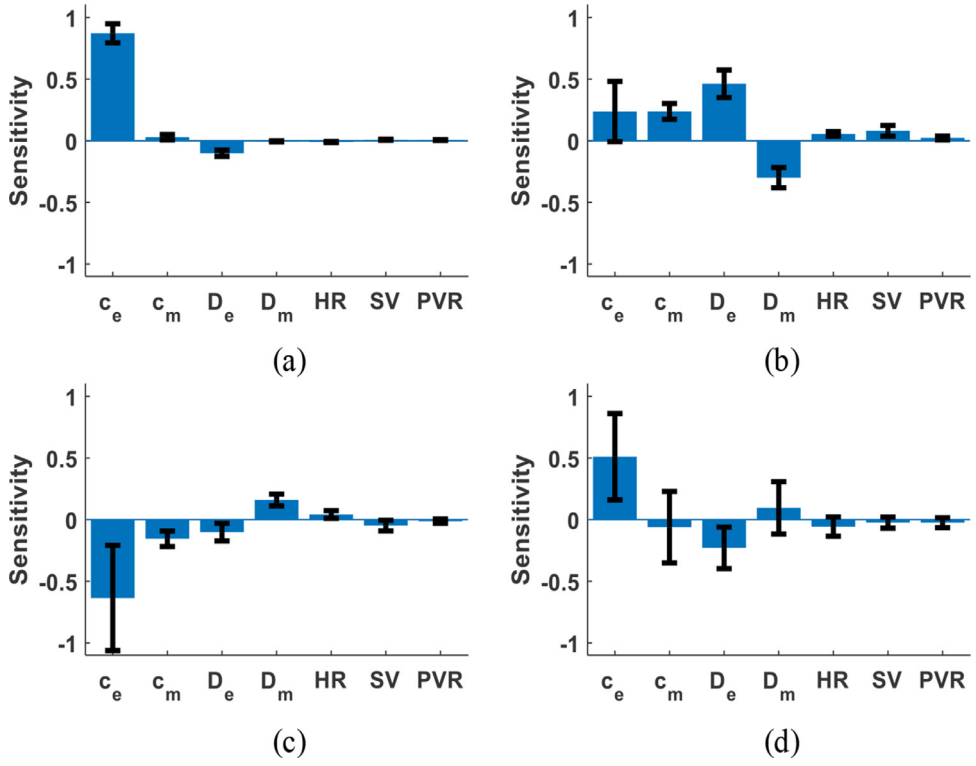

Fig. 8. Sensitivity analysis of pulse wave features versus some of the basic hemodynamic variables: (a) cfPWV; (b) RM; (c) T_{fb}; (d) $R^{r,P}_{n,d}$.

body and back through the aorta to the radial artery. Therefore, the time difference T^r_{12} between the two peaks is also partially determined by the stiffness of the large arteries. The selection of $R^{r,P}_{n,d}$ ($r = 0.65$) is interesting since its correlation with cfPWV is, to the best of our knowledge, reported for the first time, and little work has been done on understanding its physiological basis or the diastolic peak of the radial pulse wave. Furthermore, this feature is not associated with the second peak of the radial pulse, which makes it easy to extract automatically.

In the numerical study, the high sensitivity of cfPWV versus aortic PWV (Fig. 8) confirms the feasibility of using cfPWV as a surrogate for aortic PWV. Other hemodynamic variables showed hardly any effect on cfPWV. The change of aortic PWV alone caused the variation (almost linear) of cfPWV over almost its full range. The sensitivity of T_{fb} versus aortic PWV was also found to be much higher than versus any other basic hemodynamic variables. RM is affected by aortic PWV, but also by other hemodynamic variables (c_m, D_e and D_m). The effect of aortic PWV on $R^{r,P}_{n,d}$ is much larger than any other hemodynamic variables. The same can be seen from the spider plots (Fig. 9). These results agree well with the association of variables $R^{r,P}_{n,d}$, T_{fb} and RM with cfPWV found in the measured data.

The sensitivity of $R^{r,P}_{n,d}$ versus aortic PWV was higher than that of $R^{a,P}_{n,d}$ (Figs. 10 and 11), in agreement with the observation that $R^{r,P}_{n,d}$ was more closely associated with cfPWV in the analysis of the measured data. The effect of all the basic hemodynamic variables on $R^{r,P}_{n,d}$ and $R^{rf,P}_{n,d}$ was similar. Additionally, $R^{r,P}_{n,d}$ and $R^{rf,P}_{n,d}$ were closely correlated ($r = 0.94$; Fig. 12), showing that the amplitude ratio of the diastolic peak and dicrotic notch are not affected by wave reflection.

Multiplying the reciprocals by the height of the body (H) did not result in much improvement in the correlation with cfPWV. Indeed, in univariate regression analysis, H/T_{fb} and $1/T_{fb}$ gave the

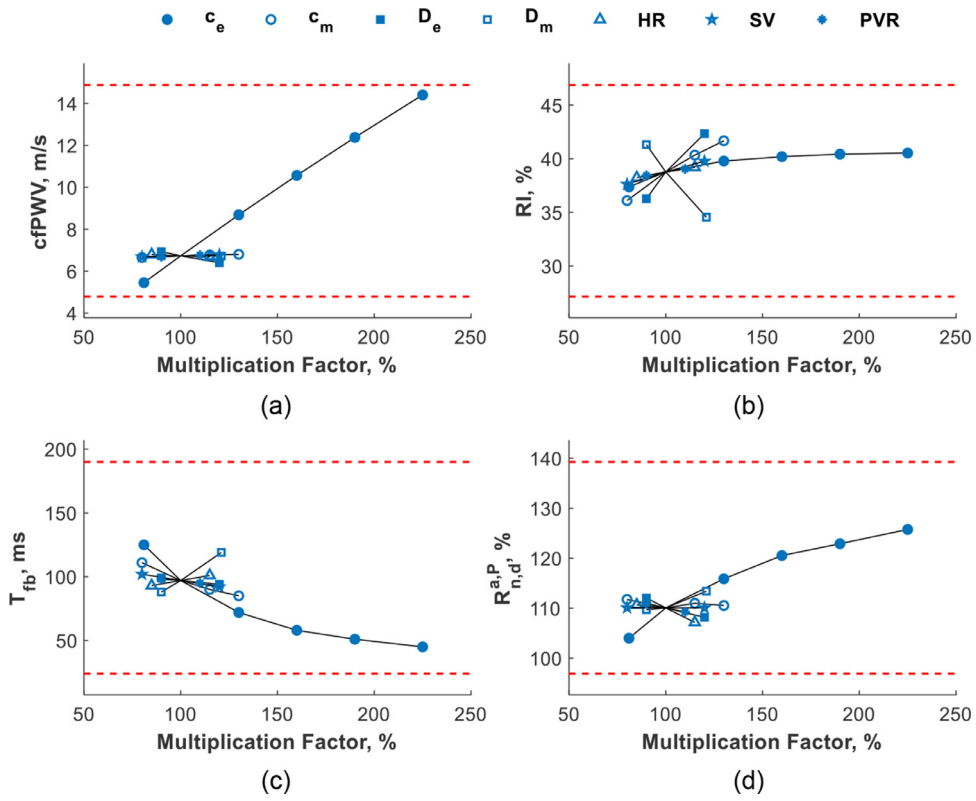

Fig. 9. Spider plot analysis of pulse wave features when the multiplication factors for all the basic hemodynamic variables of the 1-D model were equal to 100%: (a) cfPWV; (b) RM; (c) T_{fb}; (d) $R^{r,P}_{n,d}$. Red dashed lines: range of pulse wave features.

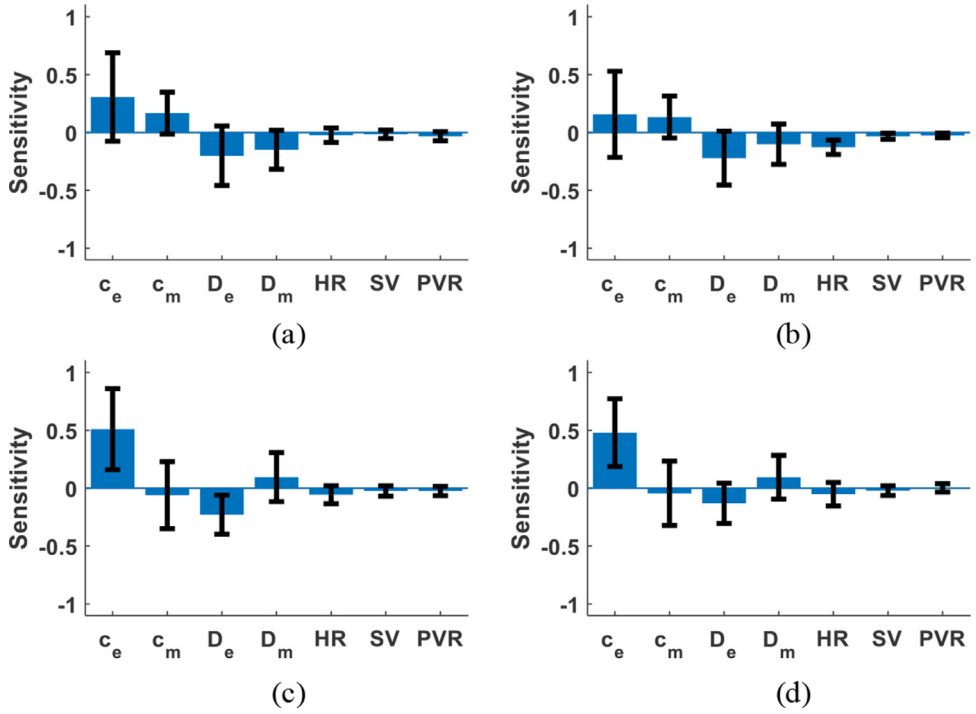

Fig. 10. Sensitivity analysis of $R^{P}_{n,d}$ calculated from different pulse waves versus all basic hemodynamic variables: (a) $R^{a,P}_{n,d}$; (b) $R^{af,P}_{n,d}$; (c) $R^{r,P}_{n,d}$; (d) $R^{rf,P}_{n,d}$.

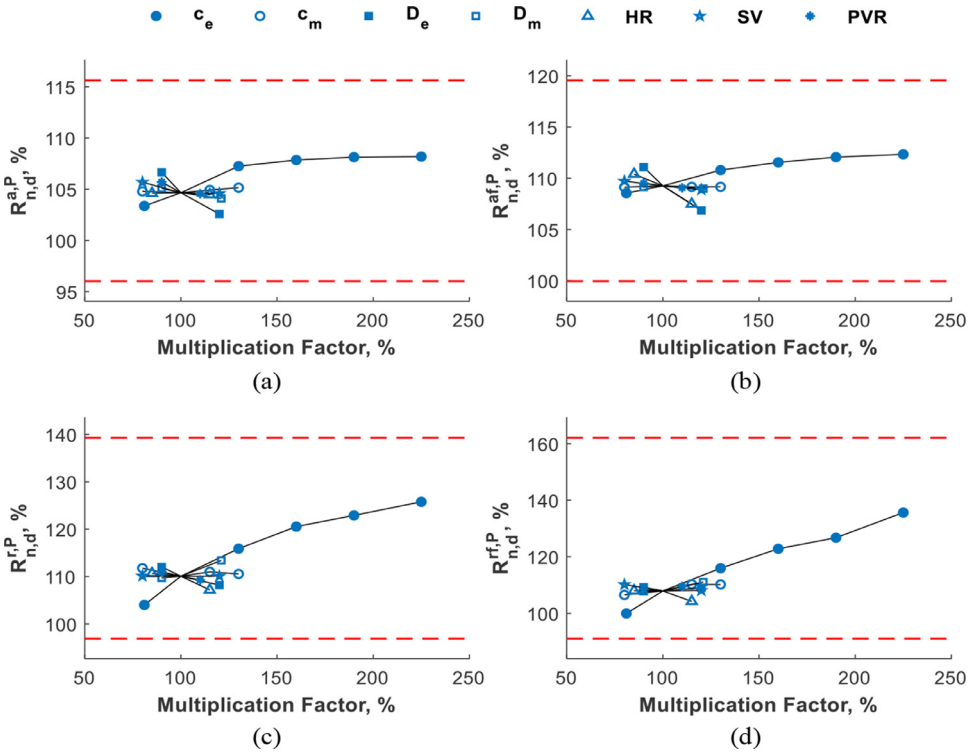

Fig. 11. Spider plot analysis of the amplitude ratio between the diastolic peak and the notch calculated from different pulse waves versus basic hemodynamic variables: (a) aortic pulse wave ($R^{a,P}_{n,d}$); (b) aortic forward wave ($R^{af,P}_{n,d}$); (c) radial pulse wave ($R^{r,P}_{n,d}$); (d) radial forward wave ($R^{rf,P}_{n,d}$). Red dashed lines: range of pulse wave features.

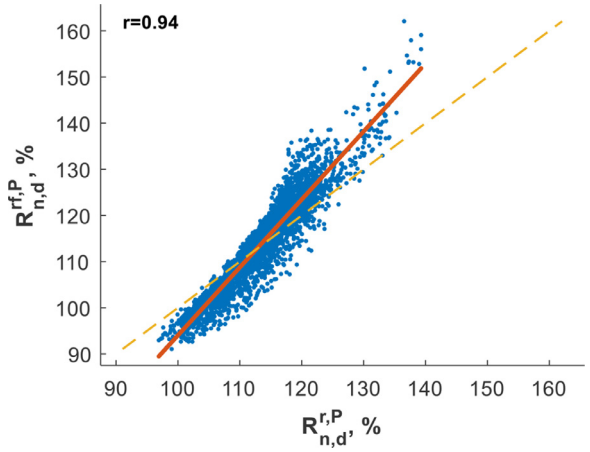

Fig. 12. Scatter plot and correlation analysis of the amplitude ratio between the diastolic peak and the notch calculated from the radial pulse wave and forward wave. Red solid line: regression between $R^{r,P}_{n,d}$ and $R^{rf,P}_{n,d}$. Orange dashed line: $R^{r,P}_{n,d}$=$R^{rf,P}_{n,d}$.

same performance in terms of correlation coefficient between the estimated and measured cfPWV, $HR^{r,P}_{n,d}$ outperformed $R^{r,P}_{n,d}$ by only 0.1, and H/T_{fb30} performed even more poorly than H/T_{fb30} (Table 3). This suggests that H may not be, or only modestly be, associated with the effective reflection distance.

4.3. Potential of radial pulse waveform to estimate cfPWV

In the validation, the regression models showed satisfactory results ($r = 0.75$, $r = 0.78$, $r = 0.79$, and $r = 0.81$; estimation error: 0 ± 1.2, -0.1 ± 1.2, -0.1 ± 1.2, and -0.1 ± 1.1 m/s for $N = 1$ to 4; Fig. 4). McHenry's select algorithm and support vector regression also produced pleasing results ($r = 0.81$ and $r = 0.80$, respectively). Therefore, we may conclude that the radial pulse waveform alone has the potential to estimate cfPWV.

Increasing the number of features included in the regression model may only modestly improve the estimation of cfPWV. The correlation coefficient between the measured cfPWV and the one estimated from features selected via McHenry's select algorithm was improved from 0.8 (when including $N = 4$ features) to 0.81, at the cost of including one more feature in the model. The support vector regression algorithm failed to outperform the all-possible regression in terms of correlation coefficient.

An inverse relationship ($r = -0.56$ for all-possible when $N = 4$, $r = -0.56$, $p < 0.001$ for McHenry's select algorithm when $N = 5$ and $r = -0.0.79$, $p < 0.001$ for support vector regression) between the estimation error and the measured value of cfPWV was found (Fig. 6 and 7, right). This may be attributed to the nonlinearity of the relation between cfPWV and the features derived from pulse wave analysis. More work is required here, which may further improve the estimation of cfPWV.

4.4. Considerations for applicability and reliability

One of the main drawbacks of the conventional AIx and the WSA technique applied in previous studies, for instance [9], is that the second peak of the radial pulse waveform or the inflection point of the aortic pulse waveform is hard to determine in some subjects. This could be addressed by the feature pairs selected in this study, which are not associated with those points. In the univariate regression analysis (Table 3), $1/T_{fb30}$, H/T_{fb30}, RM_{30}, RI_{30}, $R^{r,P}_{n,d}$ and $HR^{r,P}_{n,d}$ were neither associated with the second peak of the radial pulse waveform, nor the inflection point of the aortic pulse waveform. We removed the features that are associated with the inflection point of the aortic pulse wave and the second peak of the radial pulse wave, and applied the same analysis. The results in terms of correlation coefficient between the estimated and measured cfPWV were $r = 0.8$ for all-possible regression ($N = 4$),

$r = 0.85$ for McHenry's select algorithm, and $r = 0.84$ for support vector regression. Therefore, cfPWV may be estimated without having to deal with the difficulty of finding the second peak of the radial pulse waveform or the inflection point of the aortic pulse waveform.

4.5. Limitations and future work

All subjects were Chinese and most reported no cardiovascular conditions (115/140). Whether or not the findings apply to other ethnic groups remains to be tested. Therefore, more subjects with various cardiovascular health states should be included in future studies. The conclusion that the amplitude ratio of the diastolic peak and dicrotic notch ($R_{n,d}^{r,P}$) are not affected by wave reflection was drawn only from the numerical data. Further verification on real data is required.

The central aortic pressure waveform was calculated from the radial pressure waveform based on the transfer function method. Though evaluated on numerous cohorts, the following limitations exist: firstly, the transfer function has only been verified against the aortic pressure waveform on patients undergoing catheterization [38], not on other cohorts (e.g., healthy young men and women). A study on healthy volunteers and patients at resting state has been reported but the transfer function was verified against the carotid instead of the aortic pressure waveform [39]. Secondly, the transfer function, as a low-pass filter, may smooth out some waveform features, which could possibly be the reason that the diastolic peak cannot be extracted. Since the carotid pressure waveform can be obtained noninvasively and is closely similar in shape to the central aortic pressure waveform, future work could investigate the potential of the carotid pressure waveform in estimating cfPWV.

5. Conclusion

This study has demonstrated that (1) cfPWV can be estimated more accurately from the selected features/feature pairs of the radial and derived aortic pulse waveforms; (2) the features/feature pairs selected are physiologically interpretable; (3) some of the selected features/feature pairs are not associated with the sometimes poorly defined second peak of the radial waveform or the inflection point of the aortic waveform, and may therefore serve as more reliable and accurate substitutes for the conventional pulse wave analysis approach; (4) the ratio of the diastolic peak amplitude to the notch amplitude of the radial pulse waveform is a potential feature for cfPWV estimation and arterial stiffness assessment that is independent of wave reflections.

Conflict of interest

Appropriateness for publication: This study applied machine learning methods to the estimation of carotid-femoral pulse wave velocity (cfPWV), which is a promising research field where machine learning techniques are seldomly applied.

Backgrounds and contributions: Arterial stiffness, commonly assessed by carotid-femoral pulse wave velocity (cfPWV), is an independent biomarker for cardiovascular disease. The measurement of cfPWV, however, has been considered impractical for routine clinical application. Pulse wave analysis using a single pulse wave measurement in the radial artery is a convenient alternative. Typical methods use a single radial pulse wave feature as an estimator for cfPWV, and derived unsatisfied accuracy. In this study, we extracted various pulse wave features and applied feature selection techniques for a more accurate estimation of cfPWV from a single radial pulse wave measurement. We also found a novel diastolic radial pulse wave feature that is correlated with cfPWV, and went further to investigate the theoretical basis for this correlation using a dataset of simulated pulse waves.

We claim that this manuscript is entirely original, has not been copyrighted, published, submitted, or accepted for publication elsewhere.

Acknowledgement

The authors declare no conflict of interest. This work was supported by the National Natural Science Foundation of China under Grants 61773110 and 61701099, the Natural Science Foundation of Liaoning Province (No. 20170540312 and No. 2021-YGJC-14), the Basic Scientific Research Project (Key Project) of Liaoning Provincial Department of Education (LJKZ00042021), the Fundamental Research Funds for the Central Universities (No. N2119008). This research was also supported by the Shenyang Science and Technology Plan Fund (No. 21–104–1–24, No. 20–201–4–10, and No. 201375), the Member Program of Neusoft Research of Intelligent Healthcare Technology, Co. Ltd. (No. MCMP062002). JA acknowledged support from the British Heart Foundation (PG/15/104/31913), the Cardiovascular MedTech Cooperative at Guy's and St Thomas' NHS Foundation Trust, and the Ministry of Science and Higher Education of the Russian Federation (075–15–2020- 926).

Appendix

In this study, three sets of features were included in feature selection: (1) the raw features including subjects' general information and those extracted from time-domain, frequency-domain, and wave separation analysis; (2) the reciprocal of all the raw features; (3) all the reciprocals multiplied by body height. This appendix contains a full list of all the raw features (Table Appendix I). The 2nd and 3rd sets of features can be easily obtained from the raw features, except gender, height, cardiac cycle, and heart rate, by taking the reciprocals, and multiplying the reciprocals by body height.

Table Appendix 1
A list of features extracted for the estimation of central pulse wave velocity, along with the demographics. Note that the features gender, height, Tcardiac cycle, and heart rate were not included when generating new features by taking the reciprocal (and scaling by height; see below). Also, we used 1-AI^a instead of AI^a during this process. SEVR, Buckberg Sub-endocardial Viability Ratio. RM: reflection magnitude. RI: reflection index.

Categories	Features	Definition/calculation
General information	G #	Gender
	H #	Height
	W	Weight
	BMI	Body mass index
	T #	Cardiac cycle
	HR #	Heart rate: $60/T$
	$R_{PP}^{r,a}$	Ratio between radial and aortic pulse pressure
Time-domain features of radial pulse waveform	T_1^r	Time to the first peak
	T_2^r	Time to the second peak
	T_n^r	Time to the notch (ejection duration)
	T_d^r	Time to the diastolic peak
	T_{12}^r	$T_2^r - T_1^r$
	$R_{1,n}^{r,T}$	$T_1^r/T_n^r \times$ 100%
	$R_{2,n}^{r,T}$	$T_2^r/T_n^r \times$ 100%
	$R_n^{r,T}$	$T_n^r/T \times$ 100%
	AI^r	Radial augmentation index: $P_2^r/P_1^r \times$ 100%
	AI_d^r	$P_d^r/P_1^r \times$ 100%
	$R_{n,1}^{r,P}$	$P_n^r/P_1^r \times$ 100%
	$R_{d,n}^{r,P}$	$P_d^r/P_n^r \times$ 100%
Time-domain features of aortic pulse waveform	T_p^a	Time to the peak
	T_i^a	Time to the inflection point
	T_n^a	Time to the notch (ejection duration)
	$T_{p,i}^a$	$\lvert T_p^a - T_i^a \rvert$
	T_{dia}^a	Diastolic duration: $T - T_n^a$
	$R_{1,n}^{a,T}$	$T_1^a/T_n^a \times$ 100%
	$R_{2,n}^{a,T}$	$T_2^a/T_n^a \times$ 100%
	$R_n^{a,T}$	$T_n^a/T \times$ 100%
	$R_{dia}^{a,T}$	$T_{dia}^a/T \times$ 100%
	AI^a	Augmentation index: $(P_p^a - P_i^a)/P_p^a \times$ 100% if inflection point appears before the peak; $-(P_p^a - P_i^a)/P_p^a \times$ 100% if inflection point appears after the peak.
	$R_n^{a,P}$	$P_n^a/P_p^a \times$ 100%
	SEVR	Ratio of the area under the pressure waveform in systolic and diastolic period
Frequency-domain features of radial pulse waveform	$R_{2,1}^{r,H}$	$H_2^r/H_1^r \times$ 100%
	$R_{3,1}^{r,H}$	$H_3^r/H_1^r \times$ 100%
	$R_{4,1}^{r,H}$	$H_4^r/H_1^r \times$ 100%
	$R_{5,1}^{r,H}$	$H_5^r/H_1^r \times$ 100%
Frequency-domain features of aortic pulse waveform	$R_{2,1}^{a,H}$	$H_2^a/H_1^a \times$ 100%
	$R_{3,1}^{a,H}$	$H_3^a/H_1^a \times$ 100%
	$R_{4,1}^{a,H}$	$H_4^a/H_1^a \times$ 100%
	$R_{5,1}^{a,H}$	$H_5^a/H_1^a \times$ 100%
Wave separation features	T_{fb}	Delay between the forward and backward wave
	T_{fb30}	Delay between the forward and backward wave (using 30%T_n^a as an approximate of T_i^a)
	RI	Ratio of the backward wave amplitude to the sum of forward and backward wave amplitude
	RI_{30}	Ratio of the backward wave amplitude to the sum of forward and backward wave amplitude (using 30%T_n^a as an approximate of T_i^a)
	RM	Amplitude ratio of backward wave to the forward wave
	RM_{30}	Amplitude ratio of backward wave to the forward wave (using 30%T_n^a as an approximate of T_i^a)

Superscripts 'a' and 'r' denote features from the aortic and radial pulse waveforms, respectively. #: these features were not included when taking the reciprocal or multiplying the reciprocal by body height.

References

[1] C. Vlachopoulos, K. Aznaouridis, C. Stefanadis, Prediction of cardiovascular events and all-cause mortality with arterial stiffness: a systematic review and meta-analysis, J. Am. Coll. Cardiol. 55 (2010) 1318–1327.

[2] Y. Ben-Shlomo, M. Spears, C. Boustred, M. May, S.G. Anderson, E.J. Benjamin, P. Boutouyrie, J. Cameron, C.H. Chen, J.K. Cruickshank, S.J. Hwang, E.G. Lakatta, S. Laurent, J. Maldonado, G.F. Mitchell, S.S. Najjar, A.B. Newman, M. Ohishi, B. Pannier, T. Pereira, R.S. Vasan, T. Shokawa, K. Sutton-Tyrell, F. Verbeke, K.L. Wang, D.J. Webb, T. Willum Hansen, S. Zoungas, C.M. McEniery, J.R. Cockcroft, I.B. Wilkinson, Aortic pulse wave velocity improves cardiovascular event prediction: an individual participant meta-analysis of prospective observational data from 17,635 subjects, J. Am. Coll. Cardiol. 63 (2014) 636–646.

[3] F. Mitchell Gary, S.-J. Hwang, S. Vasan Ramachandran, G. Larson Martin, J. Pencina Michael, M. Hamburg Naomi, A. Vita Joseph, D. Levy, J. Benjamin Emelia, Arterial stiffness and cardiovascular events: the Framingham Heart Study, Circulation 121 (2010) 505–511.

[4] S. Laurent, J. Cockcroft, L. Van Bortel, P. Boutouyrie, C. Giannattasio, D. Hayoz, B. Pannier, C. Vlachopoulos, I. Wilkinson, H. Struijker-Boudier, Expert consensus document on arterial stiffness: methodological issues and clinical applications, Eur. Heart J. 27 (2006) 2588–2605.

[5] L.M. Van Bortel, S. Laurent, P. Boutouyrie, P. Chowienczyk, J. Cruickshank, T. De Backer, J. Filipovsky, S. Huybrechts, F.U. Mattace-Raso, A.D. Protogerou, Expert consensus document on the measurement of aortic stiffness in daily practice using carotid-femoral pulse wave velocity, J. Hypertens. 30 (2012) 445–448.

[6] R.R. Townsend, I.B. Wilkinson, E.L. Schiffrin, A.P. Avolio, J.A. Chirinos, J.R. Cockcroft, K.S. Heffernan, E.G. Lakatta, C.M. McEniery, G.F. Mitchell, Recommendations for improving and standardizing vascular research on arterial stiffness: a scientific statement from the American Heart Association, Hypertension 66 (2015) 698–722.

[7] B. Williams, G. Mancia, W. Spiering, E. Agabiti Rosei, M. Azizi, M. Burnier, D.L. Clement, A. Coca, G. De Simone, A. Dominiczak, 2018 ESC/ESH Guidelines for the management of arterial hypertension, Eur. Heart J. 39 (2018) 3021–3104.

[8] W.W. Nichols, Clinical measurement of arterial stiffness obtained from noninvasive pressure waveforms, Am. J. Hypertens. 18 (2005) 3s–10s.

[9] A. Qasem, A. Avolio, Determination of aortic pulse wave velocity from waveform decomposition of the central aortic pressure pulse, Hypertension 51 (2008) 188–195.

[10] S.S. Hickson, W.W. Nichols, B.J.McDonnell Yasmin, J.R. Cockcroft, I.B. Wilkinson, C.M. McEniery, A.S.I. on behalf of the, Influence of the central-to-peripheral arterial stiffness gradient on the timing and amplitude of wave reflections, Hypertens. Res. 39 (2016) 723–729.
[11] C.-.H. Chen, E. Nevo, B. Fetics, P.H. Pak, F.C. Yin, W.L. Maughan, D.A. Kass, Estimation of central aortic pressure waveform by mathematical transformation of radial tonometry pressure, Circulation 95 (1997) 1827–1836.
[12] F. Faul, E. Erdfelder, A.-.G. Lang, A. Buchner, G* Power 3: a flexible statistical power analysis program for the social, behavioral, and biomedical sciences, Behav. Res. Methods 39 (2007) 175–191.
[13] F. Faul, E. Erdfelder, A. Buchner, A.-.G. Lang, Statistical power analyses using G* Power 3.1: tests for correlation and regression analyses, Behav. Res. Methods 41 (2009) 1149–1160.
[14] G. London, A. Guerin, B. Pannier, S. Marchais, A. Benetos, M. Safar, Increased systolic pressure in chronic uremia: role of arterial wave reflections, Hypertension 20 (1992) 10–19.
[15] S. Mallat, A wavelet tour of signal processing, Academic press 1999.
[16] L. Xu, D. Zhang, K. Wang, Wavelet-based cascaded adaptive filter for removing baseline drift in pulse waveforms, IEEE Trans. Biomed. Eng. 52 (2005) 1973–1975.
[17] R. Mukkamala, J.-.O. Hahn, O.T. Inan, L.K. Mestha, C.-.S. Kim, H. Töreyin, S. Kyal, Toward ubiquitous blood pressure monitoring via pulse transit time: theory and practice, IEEE Trans. Biomed. Eng. 62 (2015) 1879–1901.
[18] G. Zhang, M. Gao, D. Xu, N.B. Olivier, R. Mukkamala, Pulse arrival time is not an adequate surrogate for pulse transit time as a marker of blood pressure, J. Appl. Physiol. 111 (2011) 1681–1686.
[19] M.F. O'Rourke, T. Yaginuma, Wave reflections and the arterial pulse, Arch. Intern. Med. 144 (1984) 366–371.
[20] Y. Yao, L. Hao, L. Xu, Y. Zhang, L. Qi, Y. Sun, B. Yang, F.N. van de Vosse, Y. Yao, Diastolic augmentation index improves radial augmentation index in assessing arterial stiffness, Sci. Rep. 7 (2017) 5864.
[21] W. Nichols, M. O'Rourke, C. Vlachopoulos, McDonald's Blood Flow in Arteries: theoretical, Experimental and Clinical Principles, CRC press 2011.
[22] G.D. Buckberg, D.E. Fixler, J.P. Archie, J.I. Hoffman, Experimental subendocardial ischemia in dogs with normal coronary arteries, Circ. Res. 30 (1972) 67–81.
[23] S. Greenwald, A. Carter, C. Berry, Effect of age on the in vitro reflection coefficient of the aortoiliac bifurcation in humans, Circulation 82 (1990) 114–123.
[24] B. Hametner, S. Wassertheurer, J. Kropf, C. Mayer, A. Holzinger, B. Eber, T. Weber, Wave reflection quantification based on pressure waveforms alone—Methods, comparison, and clinical covariates, Comput. Methods Programs Biomed. 109 (2013) 250–259.
[25] E. Westerhof Berend, I. Guelen, N. Westerhof, M. Karemaker John, A. Avolio, Quantification of wave reflection in the human aorta from pressure alone, Hypertension 48 (2006) 595–601.
[26] N. Westerhof, N. Stergiopulos, M.I.M. Noble, B.E. Westerhof, Wave Separation and Waveform Analysis, in: N. Westerhof, N. Stergiopulos, M.I.M. Noble, B.E. Westerhof (Eds.) Snapshots of Hemodynamics: An Aid For Clinical Research and Graduate Education, Springer International Publishing, Cham, 2019, pp. 175–183.
[27] K.O. McGraw, S.P. Wong, Forming inferences about some intraclass correlation coefficients, Psychol. Methods 1 (1996) 30.
[28] P.E. Shrout, J.L. Fleiss, Intraclass correlations: uses in assessing rater reliability, Psychol. Bull. 86 (1979) 420.
[29] D. Liljequist, B. Elfving, K. Skavberg Roaldsen, Intraclass correlation – A discussion and demonstration of basic features, PLoS One 14 (2019) e0219854.
[30] C.E. McHenry, Computation of a best subset in multivariate analysis, J. R. Stat. Soc. Ser. C-Appl. Stat. 27 (1978) 291–296.
[31] M. Willemet, P. Chowienczyk, J. Alastruey, A database of virtual healthy subjects to assess the accuracy of foot-to-foot pulse wave velocities for estimation of aortic stiffness, Am. J. Physiol.-Heart Circul. Physiol. 309 (2015) H663–H675.
[32] K.H. Parker, C. Jones, Forward and backward running waves in the arteries: analysis using the method of characteristics, J. Biomech. Eng.-Trans. ASME 112 (1990).
[33] A.I. Moens, Die Pulskurve, E.J. Brill., Leiden, The Netherlands, 1878.
[34] D. Korteweg, Ueber die Fortpflanzungsgeschwindigkeit des Schalles in elastischen Röhren, Ann. Phys. 241 (1878) 525–542.
[35] M. Saito, M. Matsukawa, T. Asada, Y. Watanabe, Noninvasive assessment of arterial stiffness by pulse wave analysis, IEEE Trans. Ultrason. Ferroelectr. Freq. Control 59 (2012) 2411–2419.
[36] W.W. Nichols, S.J. Denardo, I.B. Wilkinson, C.M. McEniery, J. Cockcroft, M.F. O'Rourke, Effects of arterial stiffness, pulse wave velocity, and wave reflections on the central aortic pressure waveform, J. Clin. Hypertens. 10 (2008) 295–303.
[37] P.H. Charlton, J. Mariscal Harana, S. Vennin, Y. Li, P. Chowienczyk, J. Alastruey, Modeling arterial pulse waves in healthy aging: a database for in silico evaluation of hemodynamics and pulse wave indexes, Am. J. Physiol.-Heart Circul. Physiol. 317 (2019) H1062–H1085.
[38] C.H. Chen, E. Nevo, B. Fetics, P.H. Pak, F.C. Yin, W.L. Maughan, D.A. Kass, Estimation of central aortic pressure waveform by mathematical transformation of radial tonometry pressure, Circulation 95 (1997) 1827–1836.
[39] D. Gallagher, A. Adji, M.F. O'Rourke, Validation of the transfer function technique for generating central from peripheral upper limb pressure waveform, Am. J. Hypertens. 17 (2004) 1059–1067.